Supplementary Materials for

Spin-Crossover Modulation via Single-Crystal to Single-Crystal Photochemical [2+2] Reaction in Hofmann-Type Frameworks

*Long-Fei Wang, Wei-Man Zhuang, Guo-Zhang Huang, Yan-Cong Chen, Jiang-Zhen Qiu, Zhao-Ping Ni, and Ming-Liang Tong**

CONTENTS

Table S1. Spin transition temperatures for **1**, **1′**, **2** and **2′**.

Compound	$T_c\downarrow$[a] / K	$T_c\uparrow$[a] / K	ΔT_c / K
1	212	215	3
1′	190	194	4
	166	169	3
2	164	167	3
	141	146	5
2′	162	162	0

Table S2. The ΔH and ΔS for **1**, **1′** and **2** calculated from the corresponding DSC data.

	$\Delta H\downarrow$ (kJ mol^{-1})	$\Delta S\downarrow$(J K mol^{-1})	$\Delta H\uparrow$(kJ mol^{-1})	$\Delta S\uparrow$(J K mol^{-1})
1	-9.6	-46.4	8.4	40.0
1′	- 4.08 ($\Delta H_1\downarrow$)	- 24.6 ($\Delta S_1\downarrow$)	4.98 ($\Delta H_1\uparrow$)	25.7 ($\Delta S_1\uparrow$)
	-6.33 ($\Delta H_2\downarrow$)	-38.3 ($\Delta S_2\downarrow$)	7.22 ($\Delta H_2\uparrow$)	42.7 ($\Delta S_2\uparrow$)
2	-4.40 ($\Delta H_1\downarrow$)	-26.8 ($\Delta S_1\downarrow$)	4.40 ($\Delta H_1\uparrow$)	26.3 ($\Delta S_1\uparrow$)
	-3.11 ($\Delta H_2\downarrow$)	-22.1 ($\Delta S_2\downarrow$)	2.66 ($\Delta H_2\uparrow$)	18.2 ($\Delta S_2\uparrow$)

Table S3. Crystallographic data for **1** at 120 K, 212 K and 260 K, and **1′** at 120 K, 178 K and 260 K.

Parameter	**1**			**1′**		
***T* [K]**	120	212	260	120	178	260
Formula	$C_{30}H_{22}Ag_2FeN_6$	$C_{30}H_{22}Ag_2FeN_6$	$C_{30}H_{22}Ag_2FeN_6$	$C_{30}H_{22}Ag_2FeN_6$	$C_{30}H_{22}Ag_2FeN_6$	$C_{30}H_{22}Ag_2FeN_6$
M_r	738.13	738.13	738.13	738.13	738.13	738.13
Crystal system	orthorhombic	orthorhombic	orthorhombic	orthorhombic	orthorhombic	orthorhombic
Space group	*P*bca	*P*bca	*P*bca	*P*bca	*P*bca	*P*bca
Wavelength [Å]	0.71073			0.71073		
***a* [Å]**	12.3342(6)	12.3352(6)	12.2648(5)	12.2405(7)	12.2235(6)	12.367(3)
***b* [Å]**	14.4997(7)	14.6220(7)	14.7116(6)	13.9694(9)	14.0648(7)	14.371(4)
***c* [Å]**	15.8603(8)	16.1726(8)	16.7500(8)	16.0892(9)	16.3631(7)	16.929(4)
V **[Å^3]**	2836.5(2)	2917.0(2)	3022.3(2)	2751.1(3)	2813.2(2)	3008.7(13)
Z	4	4	4	4	4	4
ρ_{calcd} **[g cm^{-3}]**	1.729	1.681	1.622	1.782	1.743	1.630
μ **(Mo Kα) [mm^{-1}]**	1.902	1.849	1.785	1.961	1.918	1.793
Refl. coll. / unique	22470 / 3245	24492 / 3848	24281 / 3456	52006 / 3169	52886 / 3231	51026 / 3443
R_{int}	0.0473	0.0474	0.0399	0.0863	0.0573	0.0869
R_1 **[$I > 2\sigma(I)$]**[a]	0.0364	0.0385	0.0319	0.0482	0.0515	0.0882
wR_2 **[all data]**[b]	0.0732	0.0779	0.0718	0.1054	0.1281	0.2334
Goof on F^2	1.145	1.116	1.080	1.099	1.075	1.096

[a] $R_1 = \sum||F_o| - |F_c||/\sum|F_o|$, [b] $wR_2 = [\sum w(F_o^2 - F_c^2)^2/w(F_o^2)^2]^{1/2}$.

Table S4. Crystallographic data for **2** at 120 K, 155 K and 185 K, and, **2′** at 90 K, 185 K and 300 K.

Parameter	**2**			**2′**		
***T* [K]**	120	155	185	90	185	300
Formula	$C_{28}H_{20}Ag_2FeN_8$	$C_{28}H_{20}Ag_2FeN_8$	$C_{28}H_{20}Ag_2FeN_8$	$C_{28}H_{20}Ag_2FeN_8$	$C_{28}H_{20}Ag_2FeN_8$	$C_{28}H_{20}Ag_2FeN_8$
M_r	740.11	740.11	740.11	740.11	740.11	740.11
Crystal system	monoclinic	triclinic	monoclinic	monoclinic	monoclinic	monoclinic
Space group	$P2_1/c$	P-1	$P2_1/c$	$P2_1/c$	$P2_1/c$	$P2_1/c$
Wavelength [Å]	1.54178			0.71073		
***a* [Å]**	8.6431(2)	8.6055(9)	8.5839(3)	8.1397(9)	8.1858(8)	8.296(5)
***b* [Å]**	15.4288(4)	15.7668(9)	16.1495(4)	16.1472(18)	16.4312(16)	16.684(9)
***c* [Å]**	12.7452(3)	12.7192(12)	12.6794(4)	12.4881(13)	12.5534(12)	12.654(7)
α **[°]**	90	89.779(8)	90	90	90	90
β **[°]**	126.962(2)	126.671(7)	126.348(2)	123.039(4)	122.720(3)	122.644(18)
γ **[°]**	90	92.338(6)	90	90	90	90
***V* [Å^3]**	1358.04(7)	1382.6(2)	1415.70(8)	1375.9(3)	1420.5(2)	1474.8(15)
Z	2	2	2	2	2	2
ρ_{calcd} **[g cm^{-3}]**	1.810	1.778	1.736	1.786	1.730	1.667
μ **(Cu/Mo Kα) [mm^{-1}]**	15.952	15.668	15.302	1.962	1.901	1.831
Refl. coll. / unique	7957 / 2183	13481 / 4454	9179 / 2807	12190 / 2553	12469 / 2631	12007 / 2731
R_{int}	0.0675	0.1502	0.0861	0.0868	0.0855	0.0912
R_1 **[$I > 2\sigma(I)$]**[a]	0.0433	0.0980	0.0560	0.0808	0.0841	0.0908
wR_2 **[all data]**[b]	0.1180	0.2651	0.1666	0.2156	0.2435	0.2666
Goof on F^2	1.057	1.058	1.107	1.053	1.050	1.040

[a] $R_1 = \sum||F_o| - |F_c||/\sum|F_o|$, [b] $wR_2 = [\sum w(F_o^2 - F_c^2)^2/w(F_o^2)^2]^{1/2}$.

Table S5. Selected structural parameters for **1** and **1′** at different temperatures.

Parameter	120 K	212 K	260 K
	Compound 1		
<Fe1–N>[a]	1.956	2.031	2.157
ΣFe[b]	18.32	15.76	13.79
Fe-N-C[c]	171.9	169.5	165.4
θ[d]	75.743(0)	74.667(0)	72.425(0)
Fe···Fe[e]	10.0459(4)	10.1699(4)	10.3801(4)
Fe···Fe[f]	9.5181(3)	9.5650(3)	9.5767(3)
Ag···Ag[g]	7.2944(5)	7.3535(5)	7.3989(5)
C-Ag-C[h]	170.77(14)	171.16(13)	171.72(12)
Parameter	**120 K**	**178 K**	**260 K**
	Compound 1′		
<Fe1–N>[a]	1.960	2.035	2.181
ΣFe[b]	17	15.6	10
Fe-N-C[c]	171.2	168.9	164.4
θ[d]	74.527	73.521	72.298(1)
Fe···Fe[e]	10.1081(4)	10.2123(3)	10.4825(18)
Fe···Fe[f]	9.2867(4)	9.3171(3)	9.4798(18)
Ag···Ag[g]	7.0018(7)	7.0515(7)	7.2047(24)
C-Ag-C[h]	174.3(2)	174.8(2)	175.5(4)

[a]The average Fe–N bond lengths (Å); [b]Octahedral distortion parameters (°); [c] Average Fe–N–C angles (°) within Hofmann layer; [d]Acute angle (°) between neighbouring Fe(II) sites within the Hofmann layer; [e]The Fe···Fe distance (Å) linked by $[Ag(CN)_2]^-$; [f]The shortest Fe···Fe distance (Å) between the neighbouring Hofmann layers; [g]The shortest Ag···Ag distance (Å) between the neighbouring Hofmann layers; [h]The C–Ag–C angles (°) of $[Ag(CN)_2]^-$.

Table S6. Geometrical parameters[1] of offset face-to-face π···π interactions between the aromatic rings of azastilbene ligands in **1** and **2** and edge-to-face π···π interactions between the aromatic rings of the intermolecular *rctt*-ht substituted cyclobutanes in **1′** and **2′** at different temperatures.

Parameter	1	1′	2	2′
Z[a]	3.83/3.85 <120 K> 3.91/3.89 <212 K> 4.01/4.01 <260 K>	4.56 <120 K> 4.66 <178 K> 4.87 <260 K>	3.77 <120 K> 3.87/3.81 <155 K> 3.94 <185 K>	5.22/5.13 <90 K> 5.34/5.17 <185 K> 5.41/5.32 <300 K>
β[b]	10.3/10.6 <120 K> 11.9/10.1 <212 K> 13.6/9.2 <260 K>	43.7 <120 K> 43.4 <178 K> 43.5 <260 K>	8.5 <120 K> 3.6/10.3 <155 K> 4.2 <185 K>	48.5/43.1 <90 K> 51.1/44.43 <185 K> 51.7/43.6 <300 K>
d[c]	3.47/3.41 <120 K> 3.47/3.45 <212 K> 3.40/3.60 <260 K>	—	3.49 <120 K> 3.51/3.46 <155 K> 3.51 <185 K>	—
r[d]	1.28/1.13 <120 K> 1.11/1.34 <212 K> 1.25/1.42 <260 K>	0.80 <120 K> 1.00 <178 K> 1.27 <260 K>	0.94 <120 K> 1.49/0.99 <155 K> 1.57 <185 K>	1.28/2.96 <90 K> 1.37/3.11 <185 K> 1.52/3.28 <300 K>
l[e]	—	3.01 <120 K> 3.03 <178 K> 3.13 <260 K>	—	3.65/3.30 <90 K> 3.74/3.30 <185 K> 3.87/3.45 <300 K>

[a]The *Z* parameter represents the distance (Å) between the centres of aromatic rings; [b]The *β* parameter represents the dihedral angle (°) between the measured aromatic rings; [c]The *d* parameter represents the distance (Å) between the centre of the 4-pyridyl unit and the plane of another aromatic ring; [d]The *r* parameter represents the offset distance (Å) between the centres of the aromatic rings, which is obtained from the equation $\sqrt[2]{Z^2 - d^2}$; [e]The *l* parameter represents the shortest distance (Å) between the H atoms of the aromatic ring and the centre of another aromatic ring.

Table S7. Selected structural parameters for **2** and **2′** at different temperatures.

Compound 2

Parameter	120 K	155 K	185 K
<Fe–N>[a]	1.967	<Fe1–N> 1.960 <Fe2–N> 2.165	2.174
ΣFe[b]	14.68	ΣFe1 9.6 ΣFe2 16	11.68
Fe-N-C[c]	171.6	Fe1-N-C 171.6 Fe2-N-C 163.4	164.7
θ[d]	79.118	77.787(2)	76.273
Fe···Fe[e]	10.0061(2)	10.1097(9) 10.1479(9)	10.2661(2)
Fe···Fe[f]	8.6431(2)	8.6055(9)	8.5839(3)
Ag···Ag[g]	7.1248(5)	6.9558(15)	7.1883(7)
C-Ag-C[h]	159.5(2)	155.0(5) 160.4(5)	158.2(3)
Ag-N[i]	2.628(5)	2.591(11) 2.617(12)	2.604(6)

Compound 2′

Parameter	**90 K**	**185 K**	**300 K**
<Fe1–N>[a]	1.980	2.057	2.145
ΣFe[b]	14.8	13.2	10.8
Fe-N-C[c]	172.6	170.6	168.8
θ[d]	75.436(1)	74.759(1)	74.357(3)
Fe···Fe[e]	10.2064(8)	10.3389(7)	10.4700(42)
Fe···Fe[f]	8.1397(9)	8.1858(8)	8.296(5)
Ag···Ag[g]	7.0743(14)	7.1488(15)	7.2463(43)
C-Ag-C[h]	176.8(5)	176.3(5)	175.9(6)
Ag···N[i]	3.1954(263)	3.1873(267)	3.1470(281)

[a]The average Fe–N bond lengths (Å); [b]Octahedral distortion parameters (°); [c]Average Fe–N–C angles (°) within Hofmann layer; [d]Acute angle (°) between neighbouring Fe(II) sites within the Hofmann layer; [e]The Fe···Fe distance (Å) linked by $[Ag(CN)_2]^-$; [f]The shortest Fe···Fe distance (Å) between the neighbouring Hofmann layers; [g]The shortest Ag···Ag distance (Å) between the neighbouring Hofmann layers; [h]The C–Ag–C angles (°) of $[Ag(CN)_2]^-$; [i]The distance (Å) between the Ag atom and the N atom of 3-pridyl group.

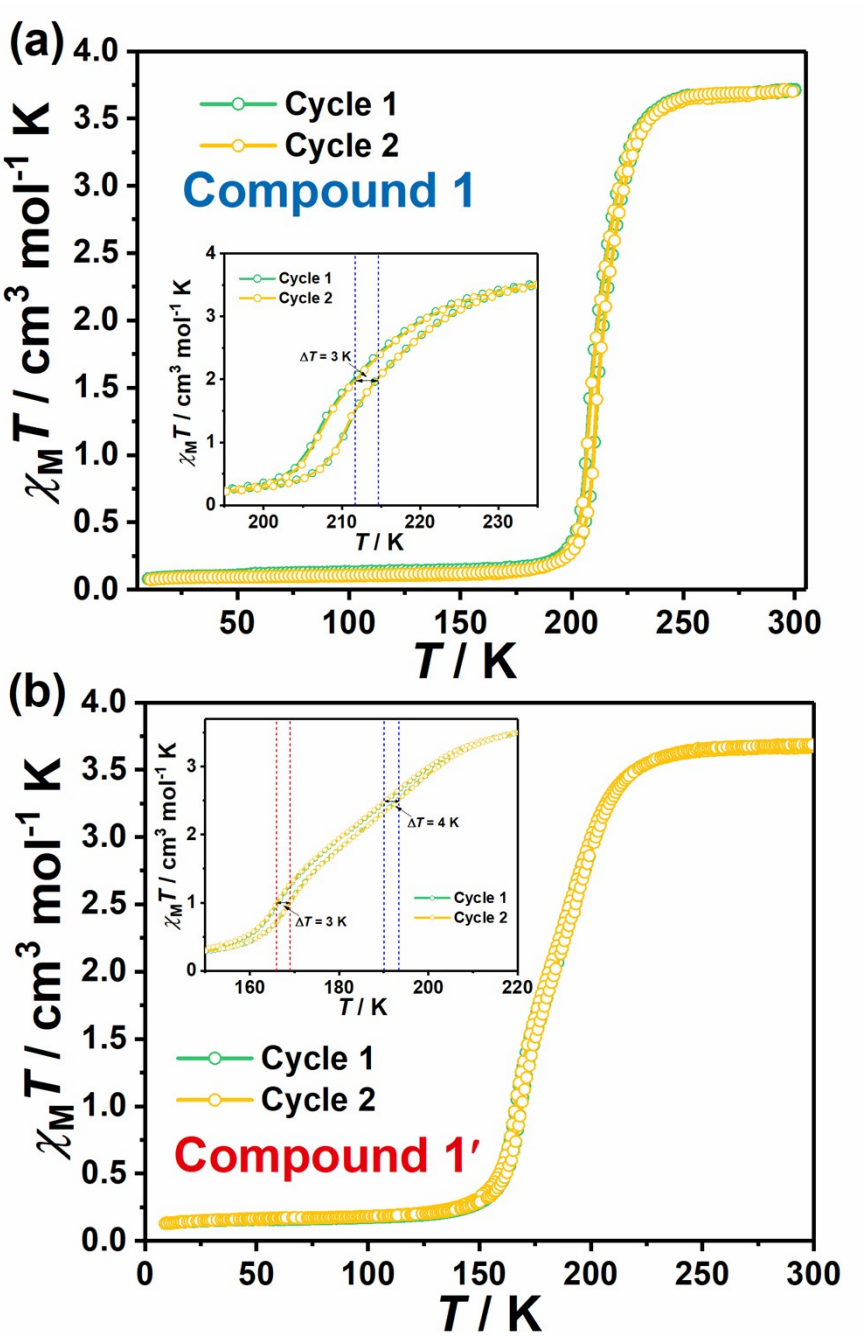

Figure S1. Variable temperature magnetic susceptibility data for **1** (a) and **1′** (b) with the scan rate of 2 K/min for 2 cycles.

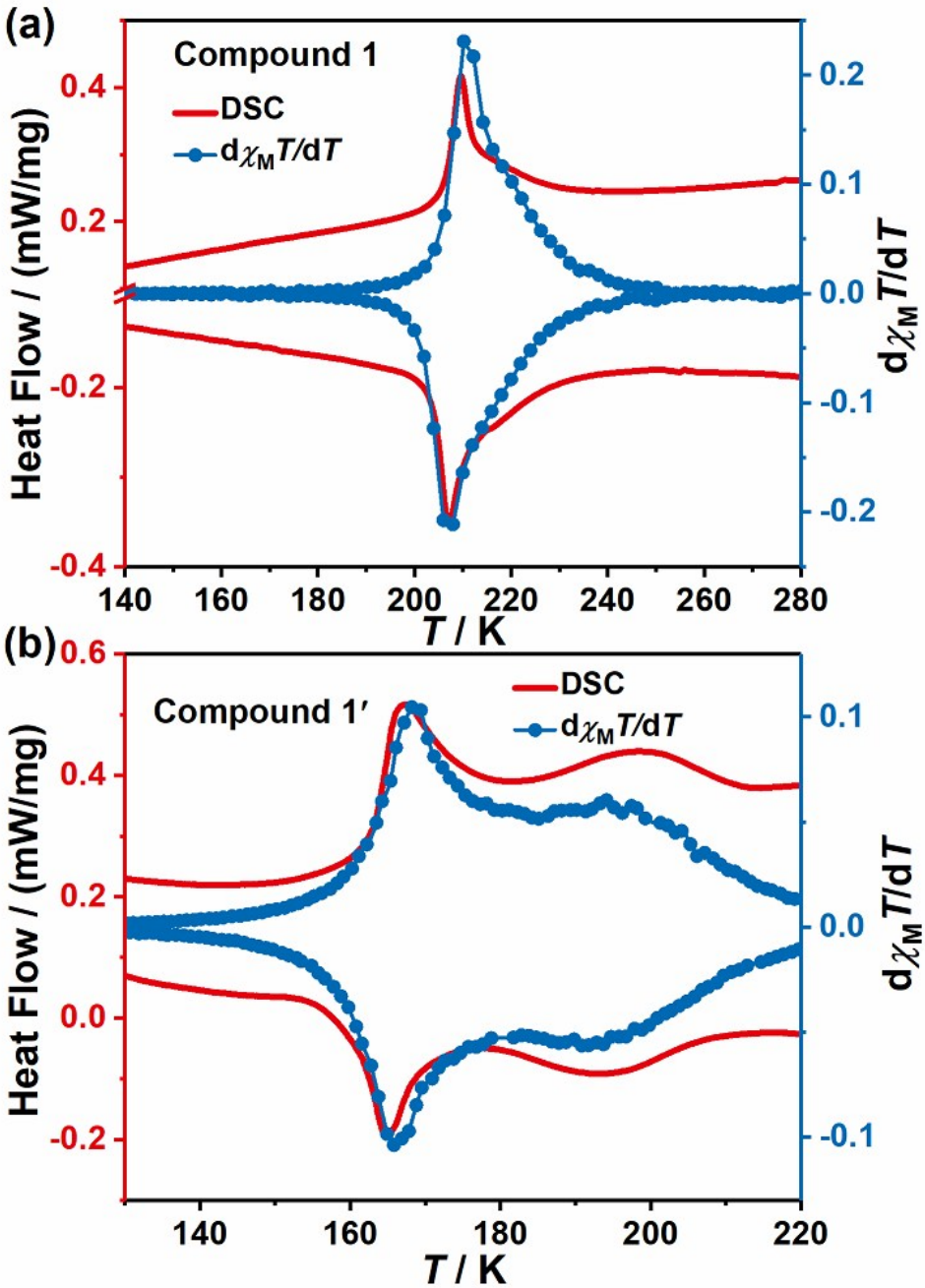

Figure S2. (a) A comparison between the DSC curve (red) and the differentiation of $\chi_M T$ versus T plot (blue) for **1**. (b) A comparison between the DSC curve (red) and the differentiation of $\chi_M T$ versus T plot (blue) for **1′**.

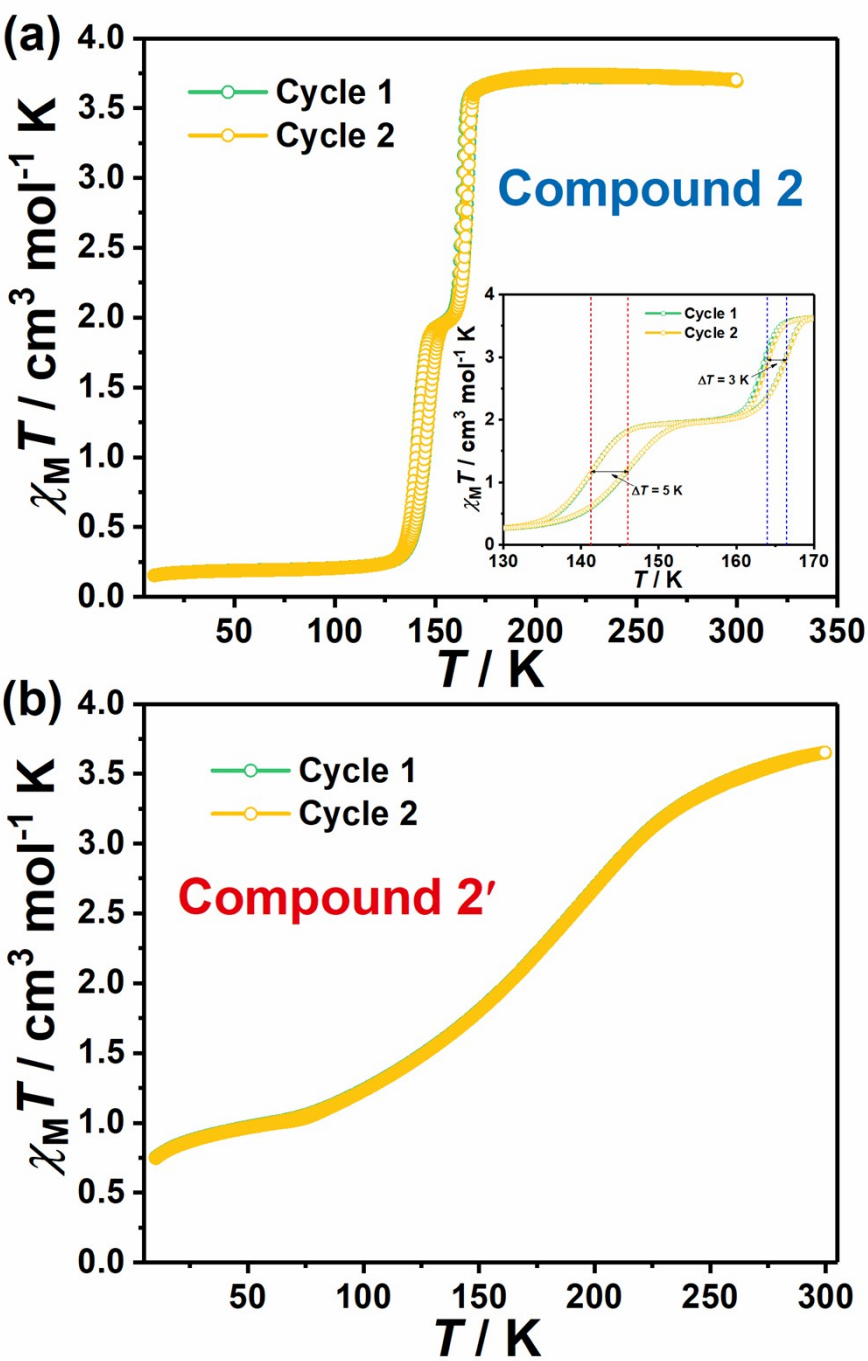

Figure S3. Variable temperature magnetic susceptibility data for **2** (a) and **2′** (b) with the scan rate of 2 K/min for 2 cycles.

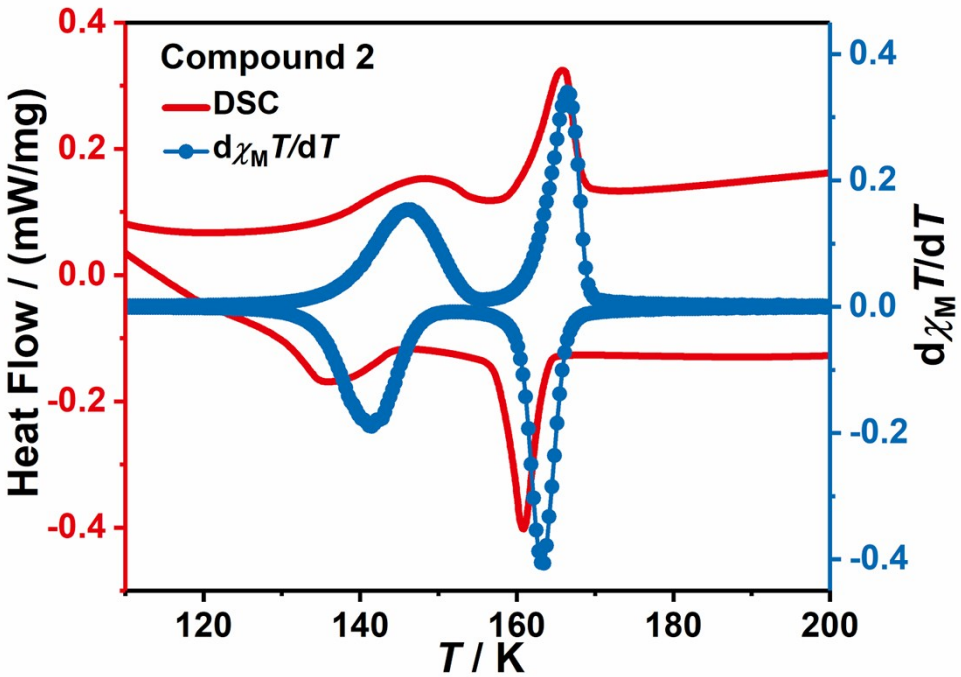

Figure S4. A comparison between the DSC curve (red) and the differentiation of $\chi_M T$ versus T plot (blue) for **2**.

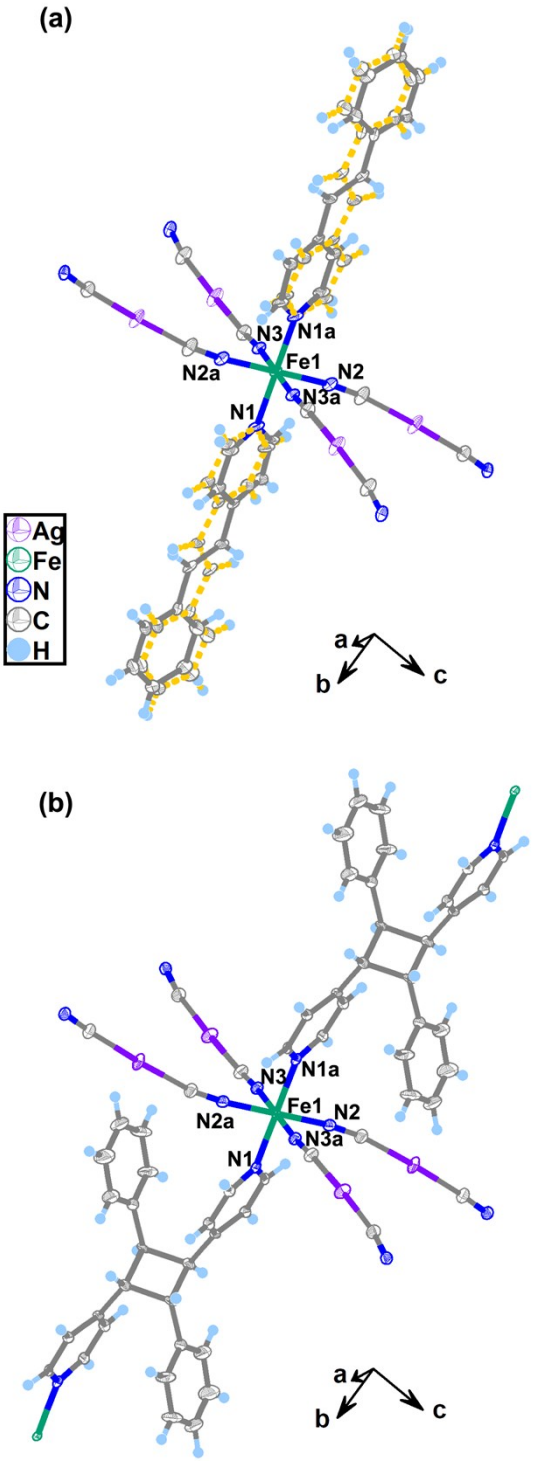

Figure S5. The ORTEP views (60% thermal ellipsoids) of the coordination environment of Fe(II) ions in **1** (a) and **1′** (b) at 120 K. Color code: Fe green; Ag purple; N blue; C gray; H light blue. Symmetry code: (a) 1-x, 2-y, 1-z.

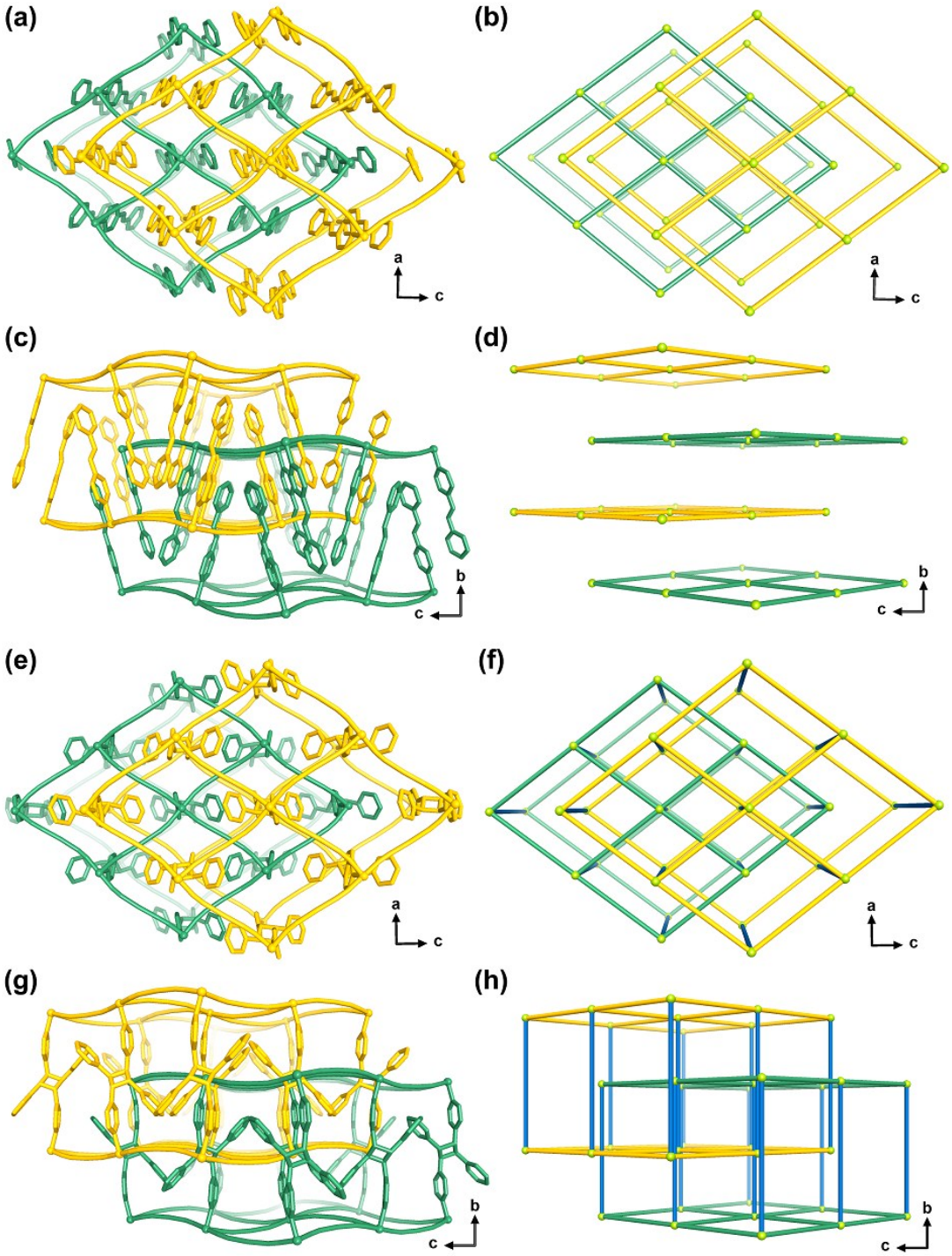

Figure S6. The views of the 2D Hofmann-type structure (a, c) and the simplified *sql* topological framework (b, d) for **1** along the *b* (a, b) and *a* (c, d) axis. The views of the 3D Hofmann-type structure (e, g) and the simplified doubly interpenetrated *pcu* topological framework (f, h) for **1′** along the *b* (e, f) and *a* (g, h) axis. The disorder part in **1** is omitted for clarity.

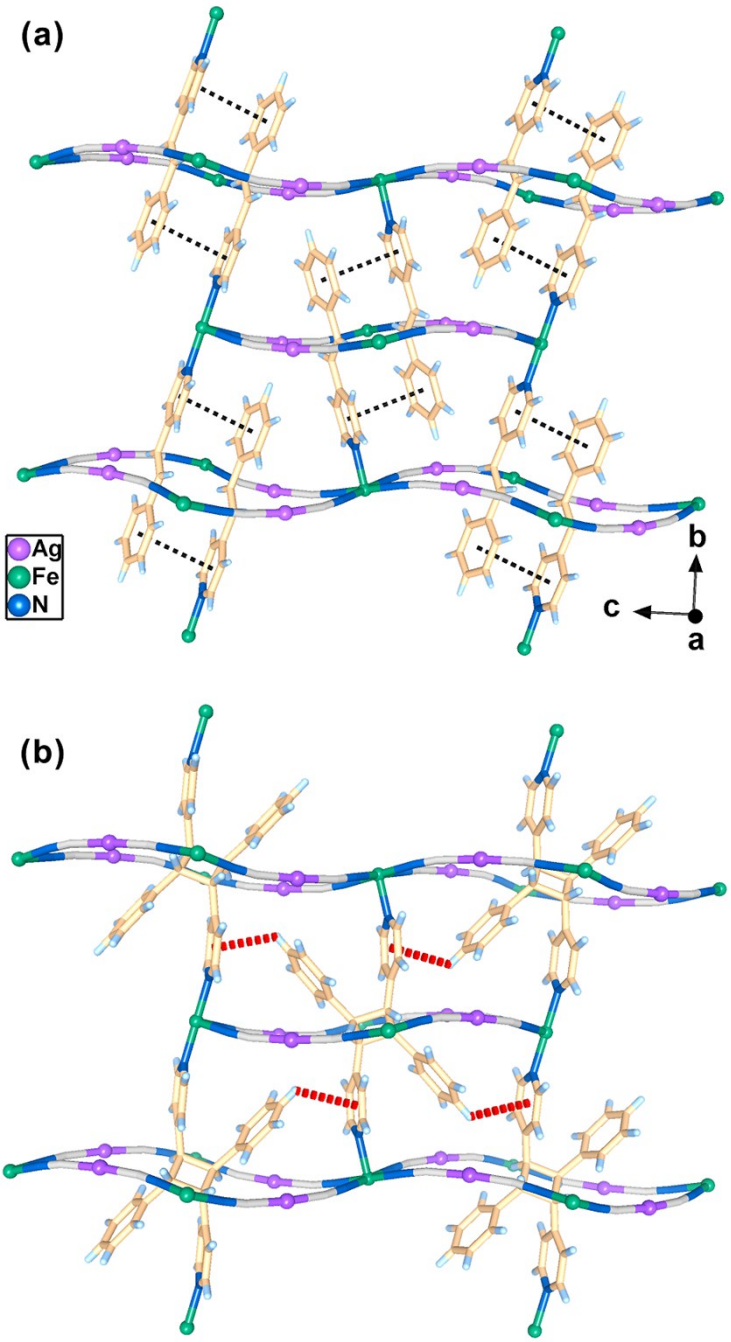

Figure S7. The views of offset face-to-face π···π interactions (black dashed line) between the aromatic rings of the paired 4-spy ligands in **1** (a) and edge-to-face π···π interactions (red dashed line) between the aromatic rings of the intermolecular *rctt*-ht substituted cyclobutanes in **1′** (b) at 260 K.

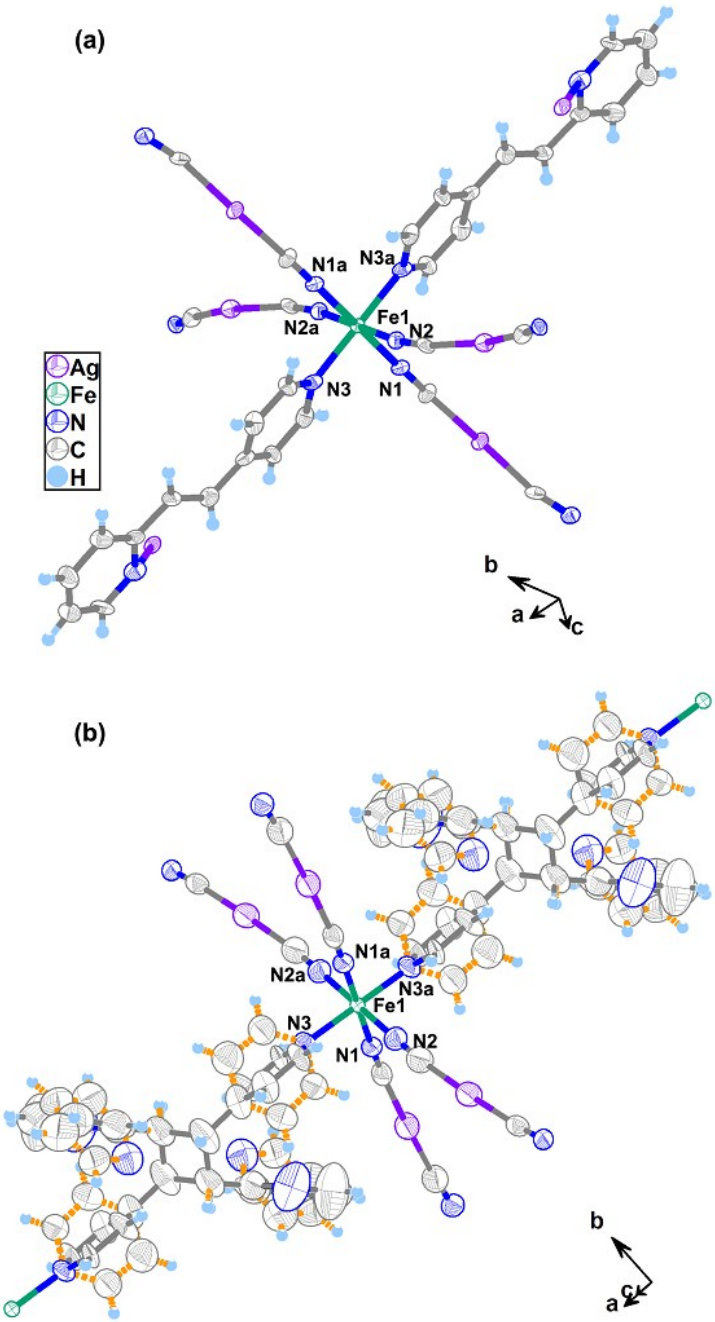

Figure S8. The ORTEP views (60% thermal ellipsoids) of the coordination environment of Fe(II) ions in **2** at 120 K and **2′** (b) at 90 K. Color code: Fe green; Ag purple; N blue; C gray; H light blue. Symmetry code: a -1/2+x, 1/2-y, -1/2+z.

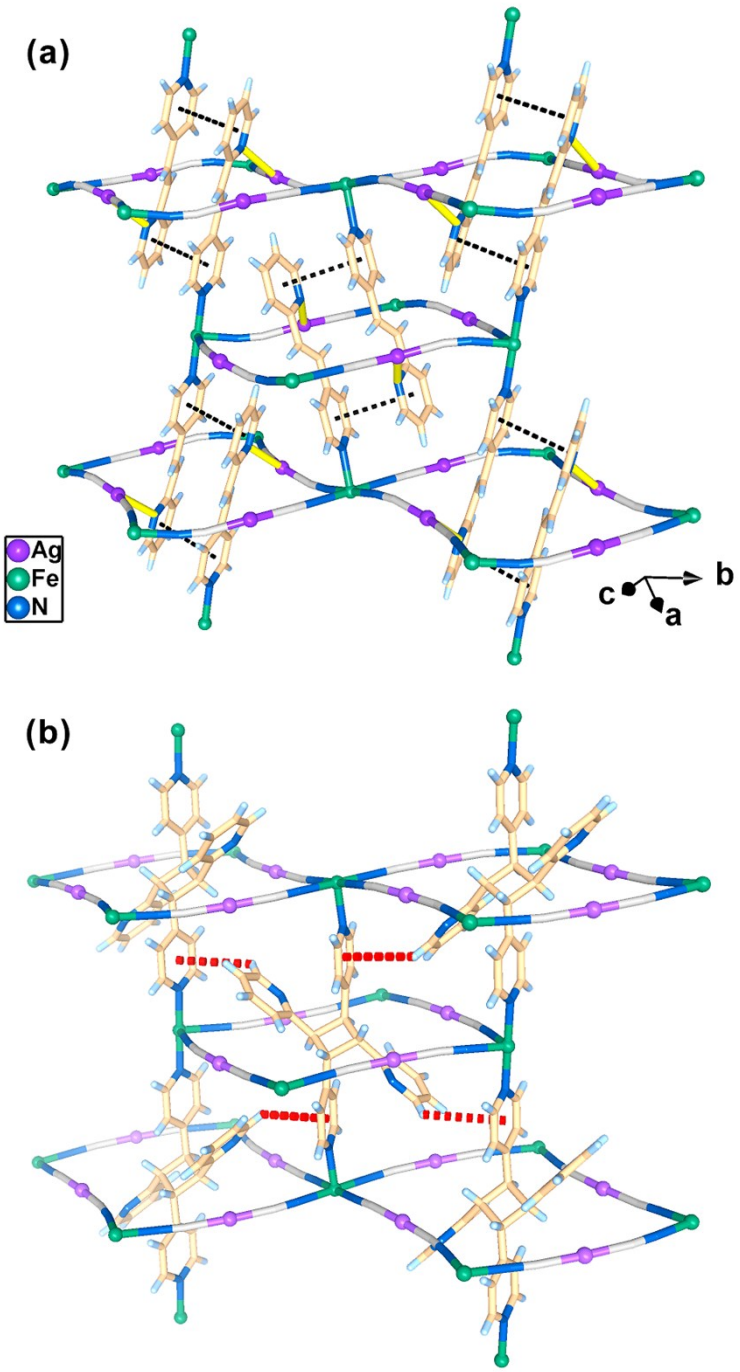

Figure S9. The views of offset face-to-face π···π interactions (black dashed line) between the aromatic rings of the paired 2,4-bpe ligands in **2** (a) at 185 K and edge-to-face π···π interactions (red dashed line) between the aromatic rings of the intermolecular *rctt*-ht substituted cyclobutanes in **2′** (b) at 300 K. The Ag(I)–N_{py} bonds are presented as yellow rods.

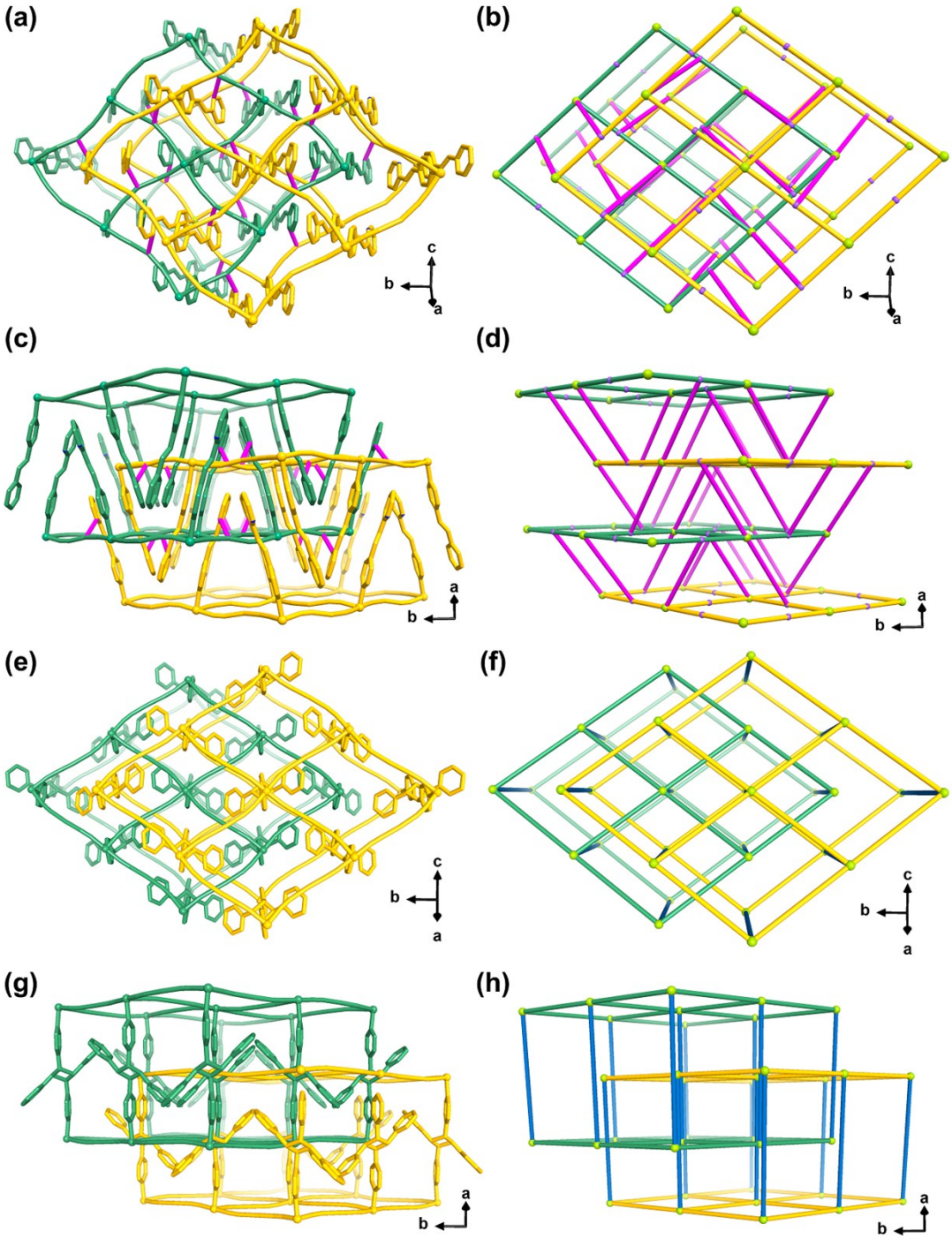

Figure S10. The top (a, b) and side views (c, d) of the 3D Hofmann-type structure (a, c) and the simplified *rtl* topological framework (b, d) for **2**. The top (e, f) and side views (g, h) of the 3D Hofmann-type structure (e, g) and the simplified doubly interpenetrated *pcu* topological framework (f, h) for **2′**.

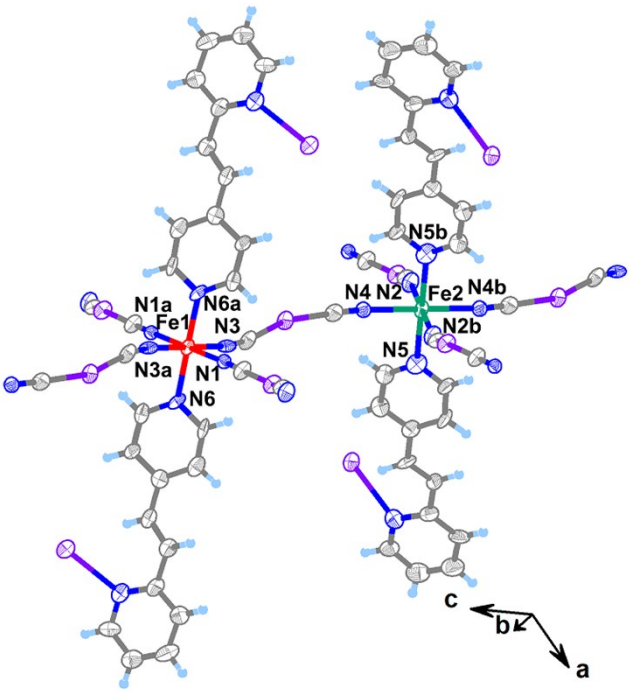

Figure S11. The ORTEP views (60% thermal ellipsoids) of the coordination environment of Fe(II) ions in **2** at 155 K. Color code: Fe1 (LS) red; Fe2 (HS) green; Ag purple; N blue; C gray; H light blue. Symmetry code: a -1-x, 1-y, 1-z; b -1-x, 1-y, -z.

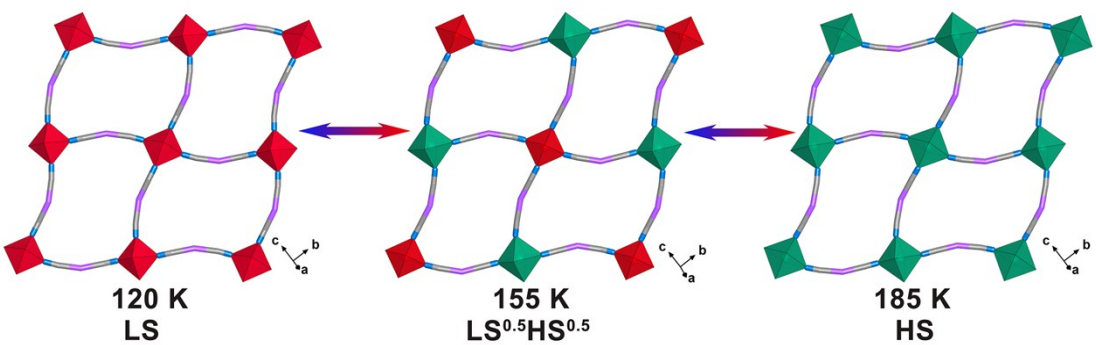

Figure S12. Schematic representation of the spin-state conversions of Fe(II) ions in the $[Fe\{Ag(CN)_2\}_2]_\infty$ layer of **2** between LS, $LS^{0.5}HS^{0.5}$ and HS states. Red and green polyhedra represent the LS and HS Fe(II) coordination spheres, respectively.

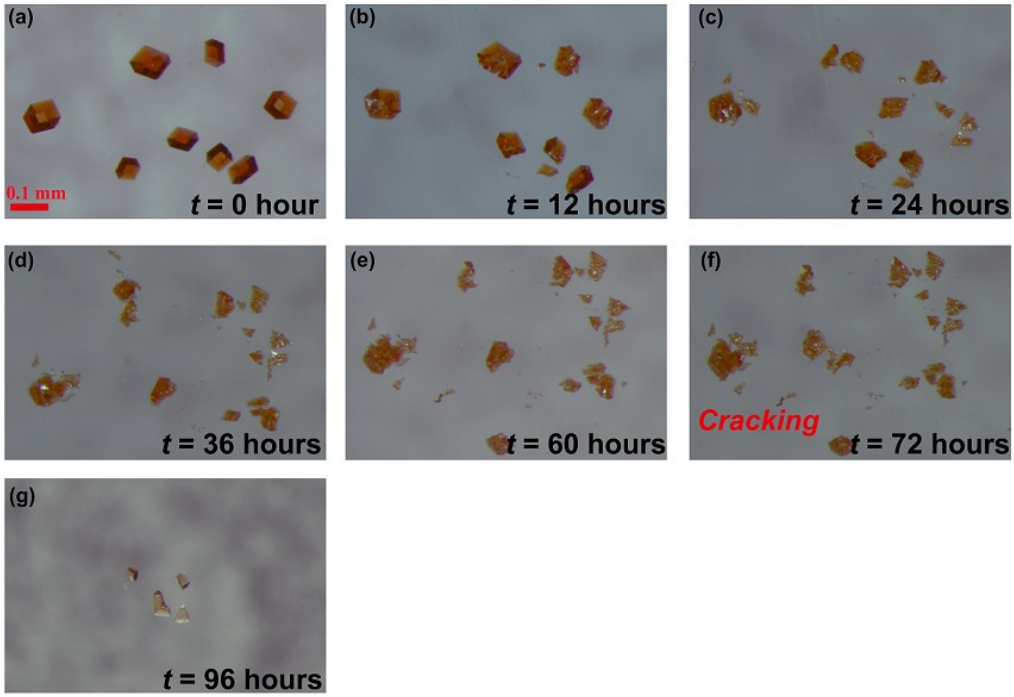

Figure S13. Single crystal pictures of **2** with different UV light irradiation time (P = 500 W), which show the gradually cracking of the crystal with the growth of irradiation time. (g) Selected fragments of the crystals of **2** with the single crystal properties after irradiated for 96 hours.

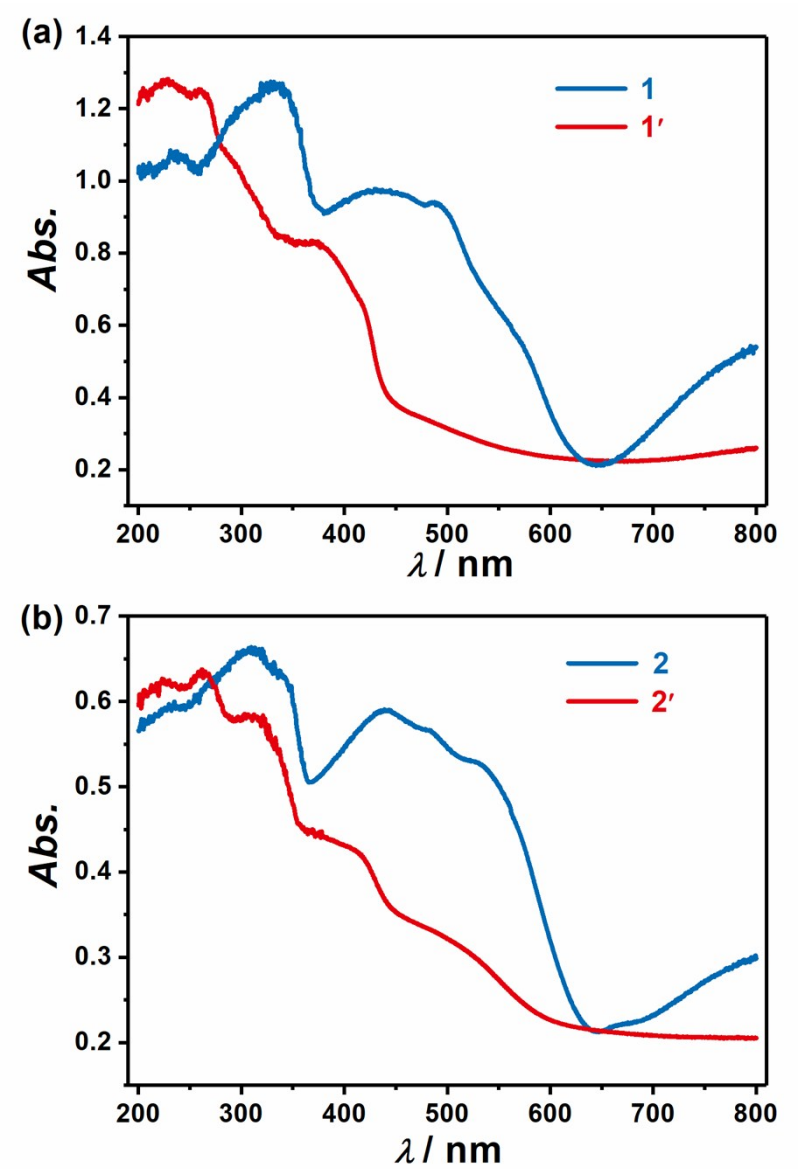

Figure S14. The UV-Vis spectrum for **1**, **1′**, **2** and **2′**.

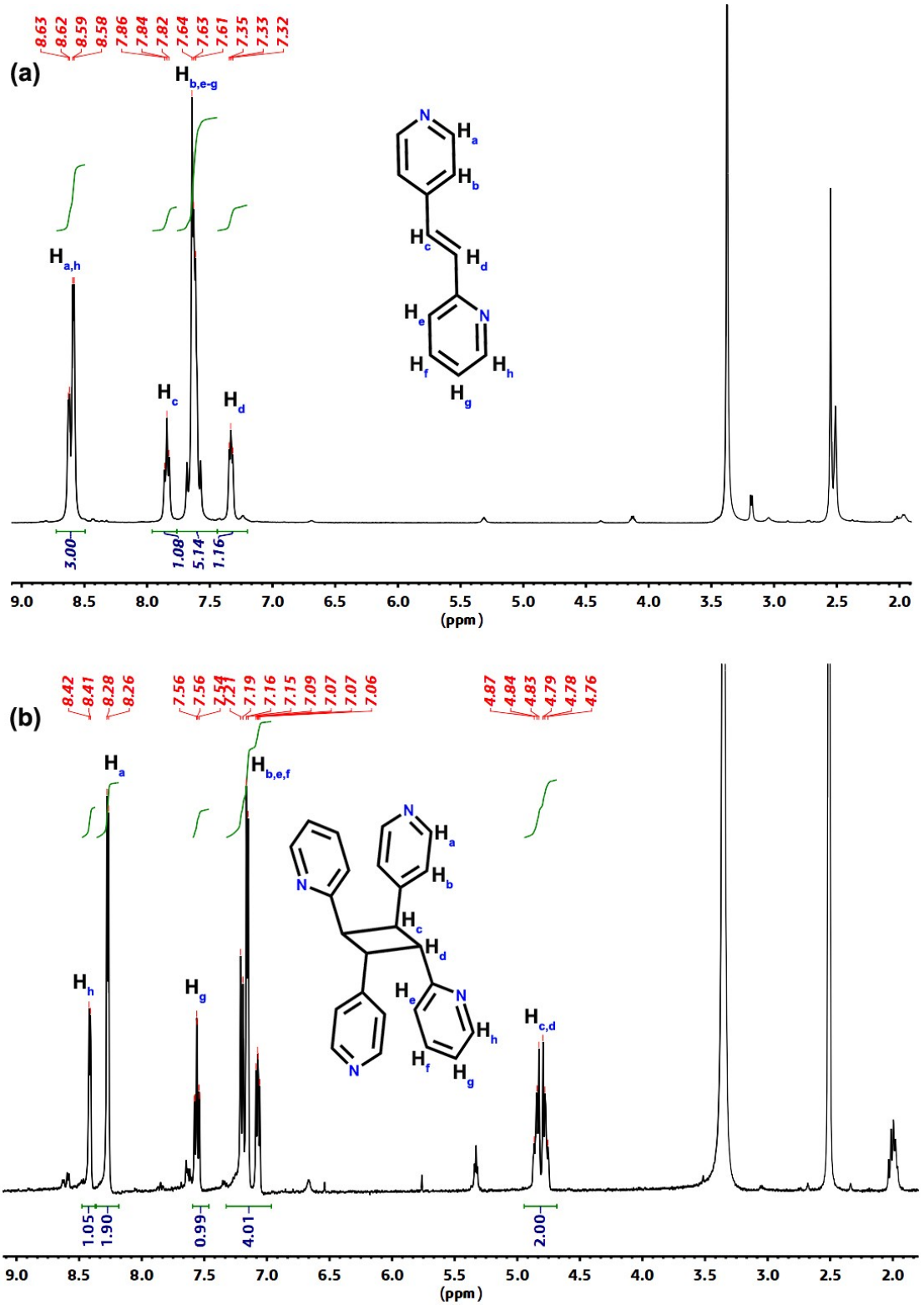

Figure S15. ^{1}H NMR spectra of the framework digestion products of **2** (a) and **2′** (b).

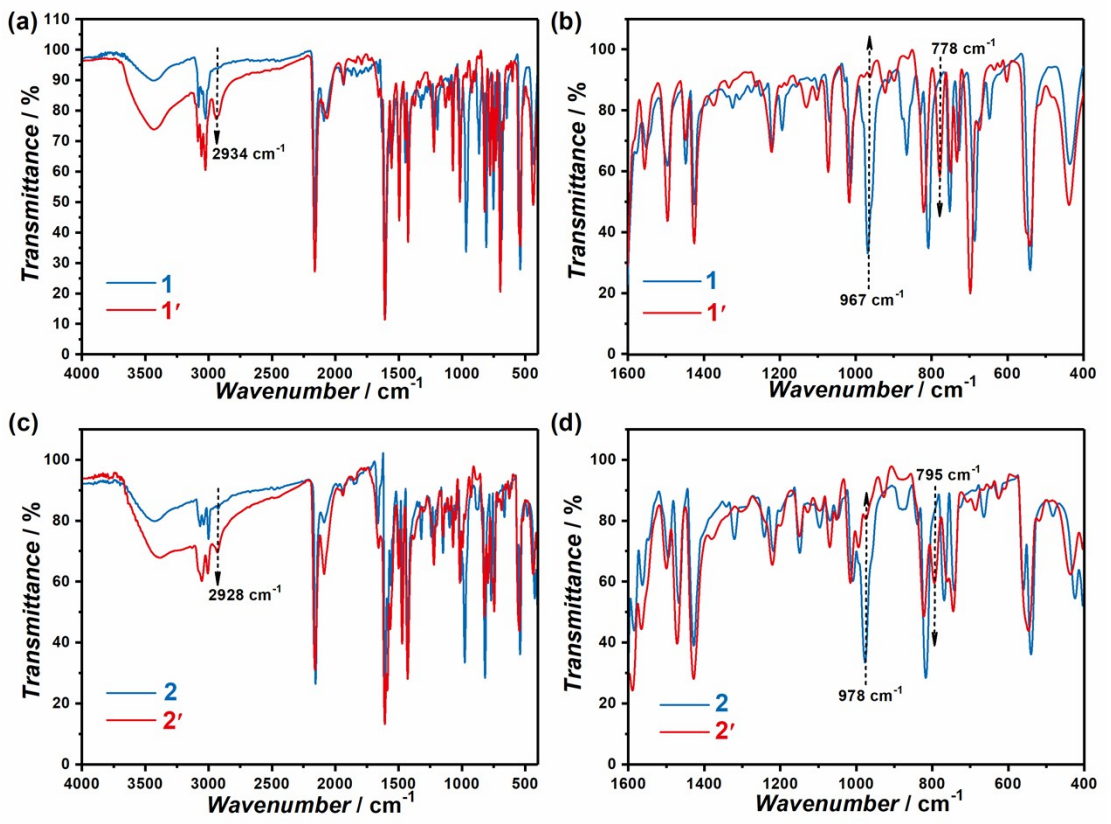

Figure S16. The IR spectra show the disappearance of the C=C-H out-of-plane bending vibrations at 967 cm^{-1} (978 cm^{-1}) for **1** (**2**) and appearance of the saturated C-H stretching vibrations at 2934 cm^{-1} (2928 cm^{-1}) for **1′** (**2′**), respectively.

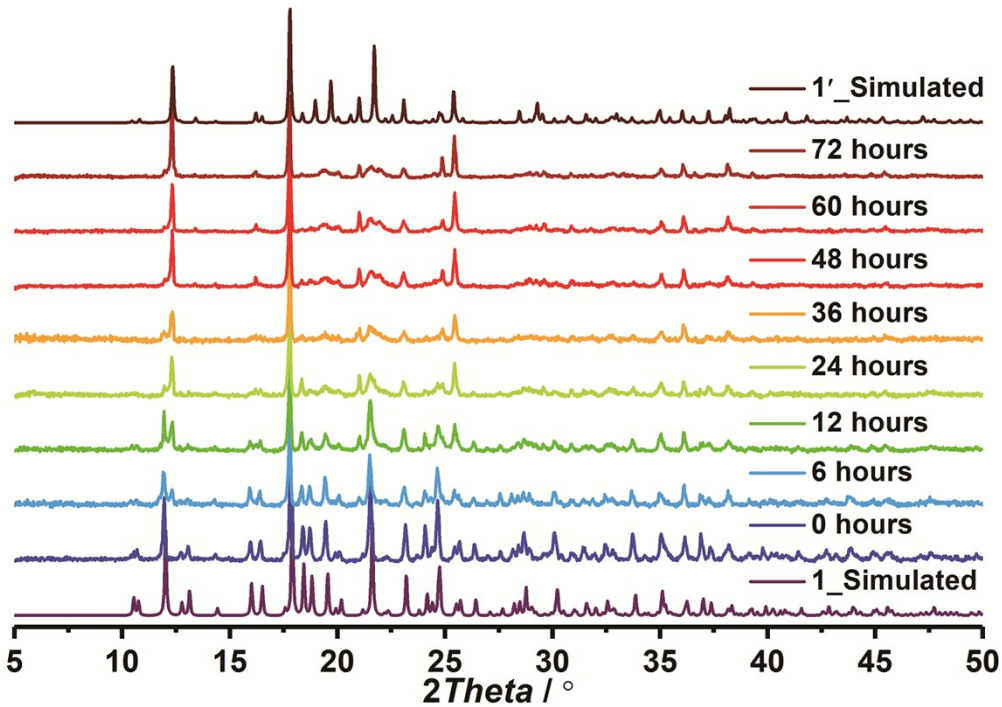

Figure S17. The Powder X-ray diffraction data plot of compound **1** at different UV light irradiation time.

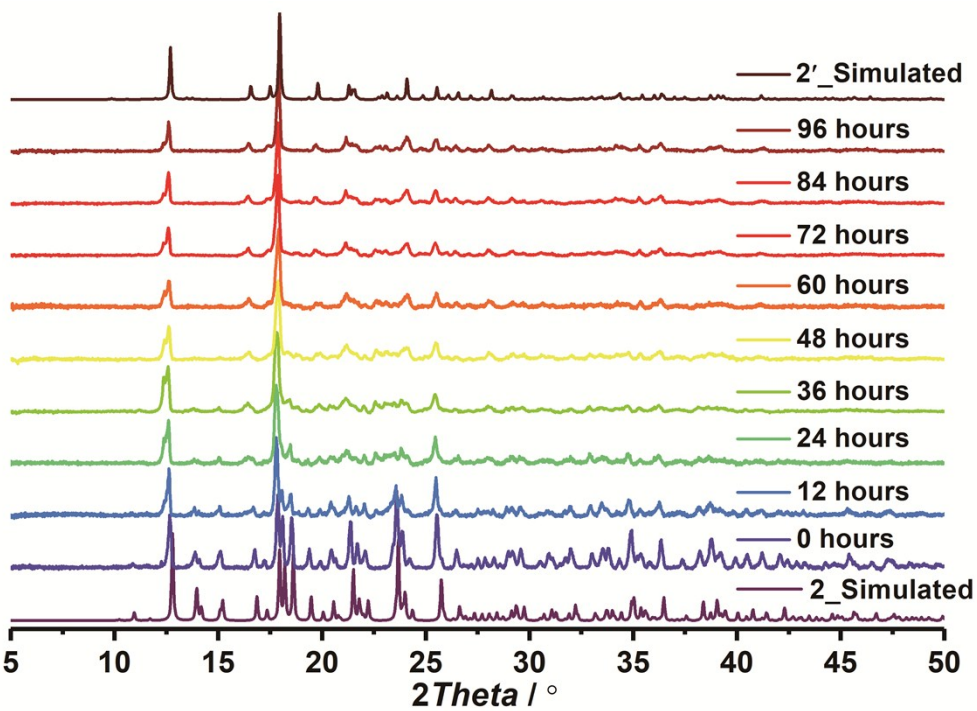

Figure S18. The Powder X-ray diffraction data plot of compound **2** at different UV light irradiation time.

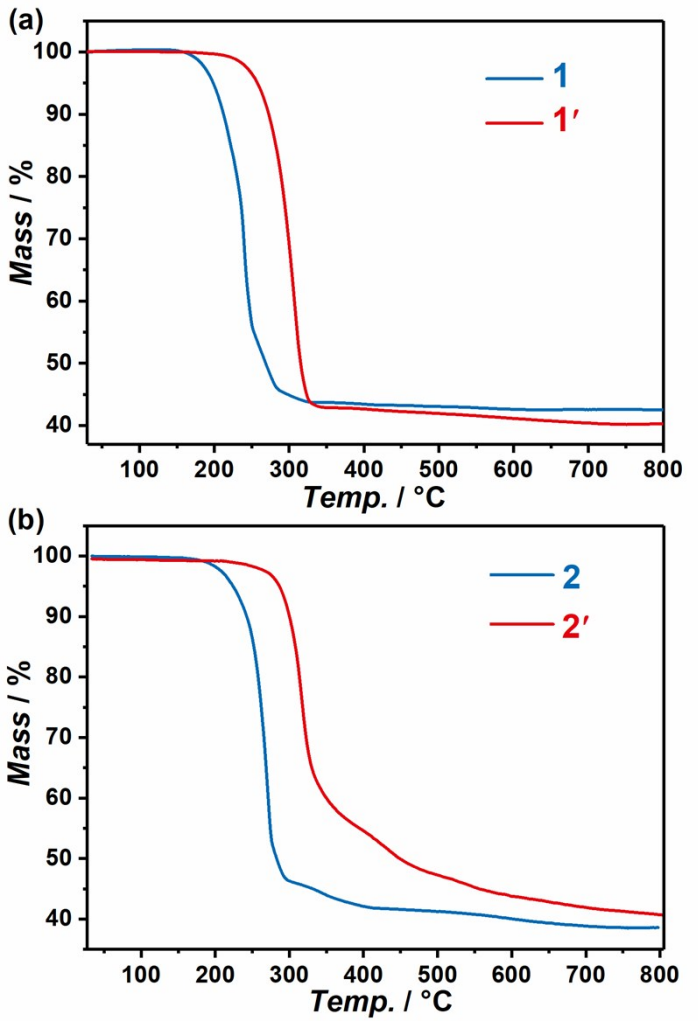

Figure S19 (a) Thermogravimetric-mass spectroscopy analyses of **1** (blue line) and **1′** (red line). (b) Thermogravimetric-mass spectroscopy analyses of **2** (blue line) and **2′** (red line).

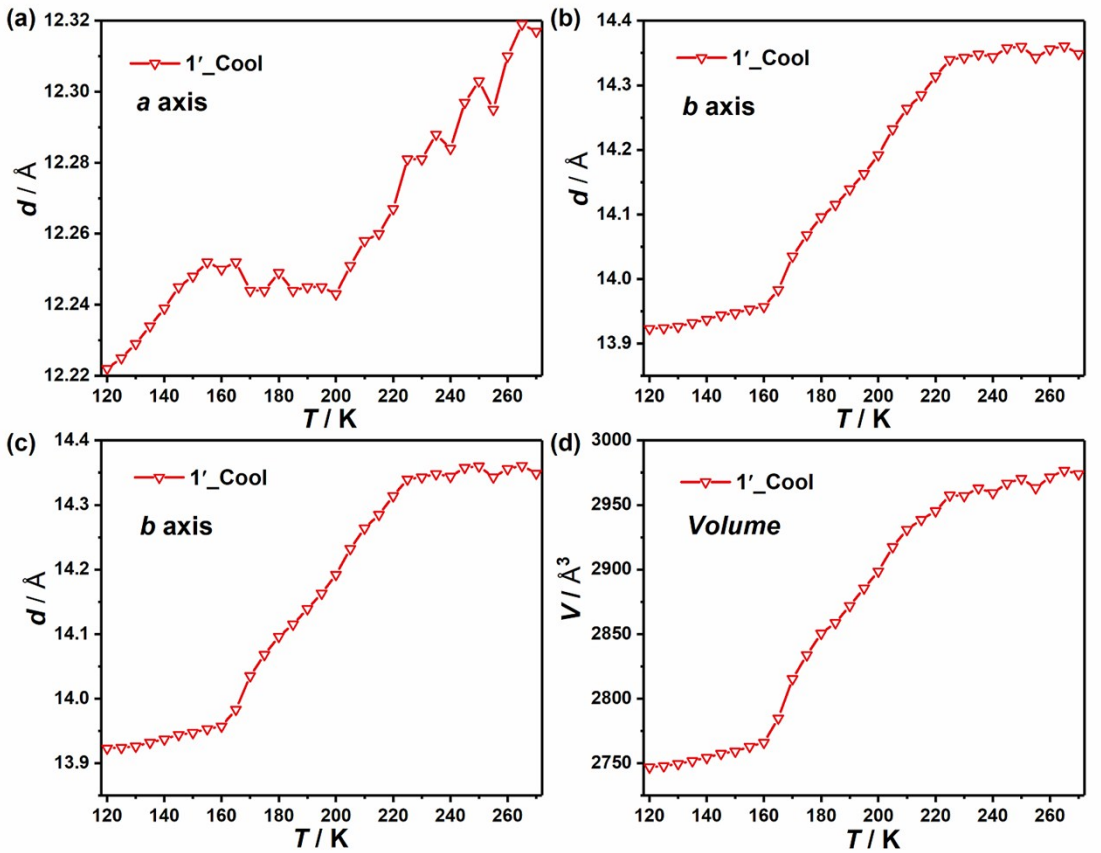

Figure S20. Variable temperature SCXRD unit cell parameters for **1′**.

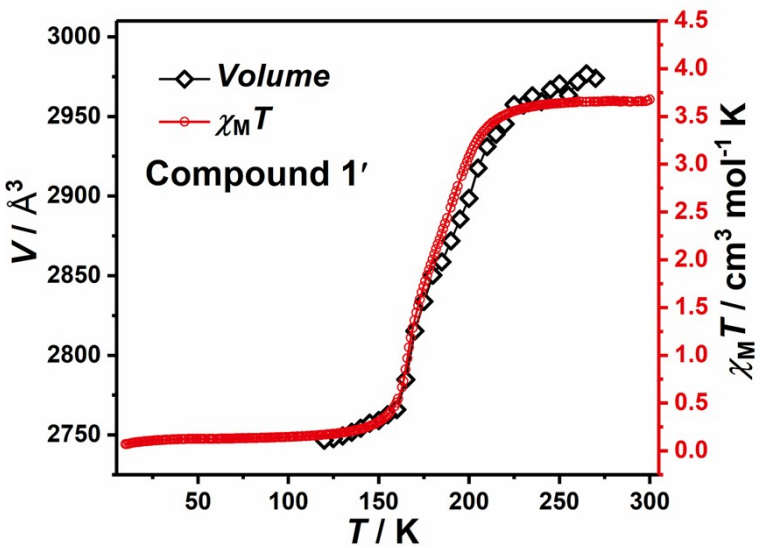

Figure S21. Magnetic susceptibility data for a bulk sample of **1′** (red) and corresponding variable temperature SCXRD unit cell Volume for **1′** (black).

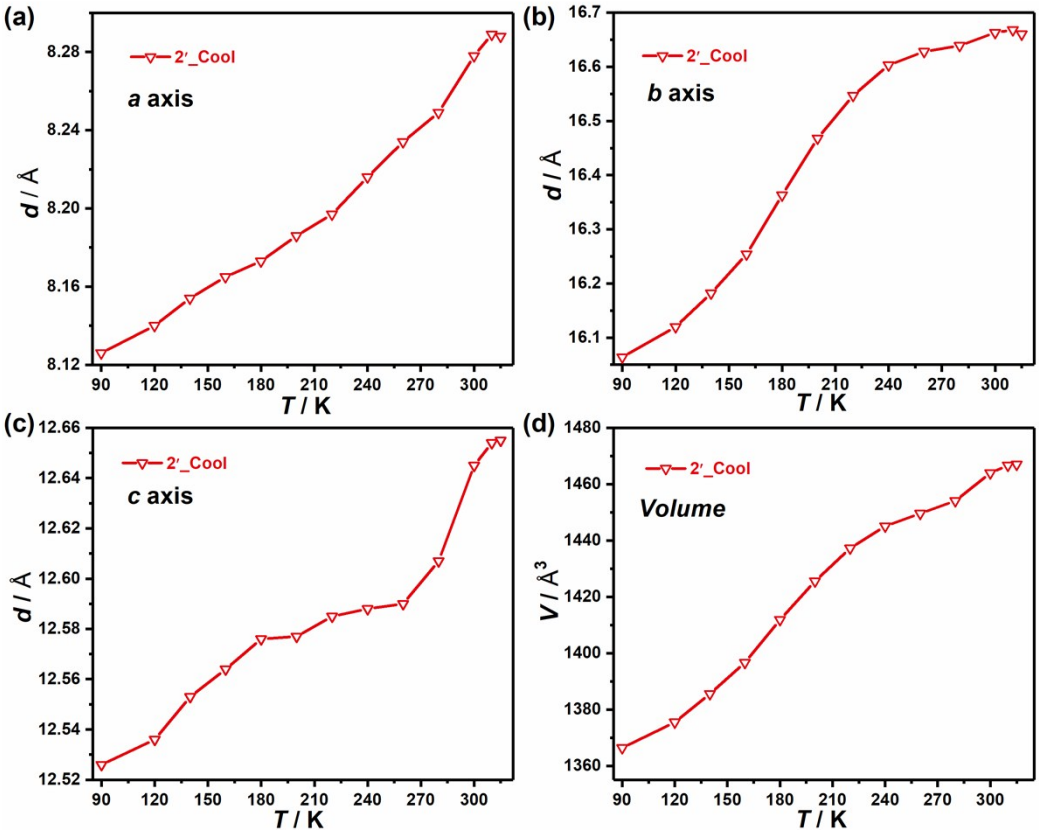

Figure S22. Variable temperature SCXRD unit cell parameters for **2′**.

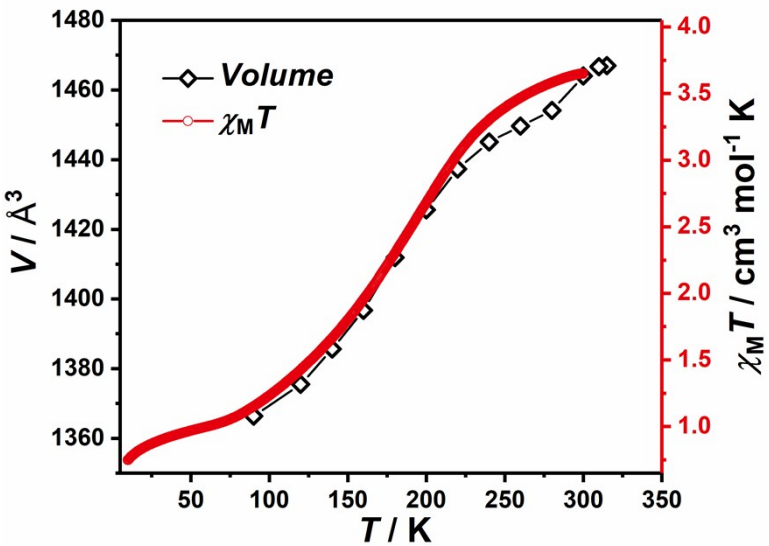

Figure S23. Magnetic susceptibility data for a bulk sample of **2′** (red) and corresponding variable temperature SCXRD unit cell Volume for **2′** (black).

Reference

[1] a) S. Tsuzuki, T. Uchimaru, K.-I. Sugawara, M. Mikami, *J. Chem. Phys.* **2002**, *117*, 11216–11221; b) R. L. Jaffe, *J. Chem. Phys.* **1996**, *105*, 2780–2788; c) S. Tsuzuki, K. Honda, T. Uchimaru, M. Mikami, K. Tanabe, *J. Am. Chem. Soc.* **2002**, *124*, 104–112.